3-2023

Antimicrobial Edible Coating Composed of Chitosan Polyvinyl Alcohol and Zinc-Coated Halloysite Nanotubes

Sindhu Datla

ANTIMICROBIAL EDIBLE COATING COMPOSED OF CHITOSAN POLYVINYL ALCOHOL AND ZINC-COATED HALLOYSITE NANOTUBES

by

Sindhu Datla, B. Pharmacy

A Thesis Presented in Partial Fulfillment
of the Requirements of the Degree
Master of Science in Molecular Sciences and Nanotechnology

COLLEGE OF ENGINEERING AND SCIENCE
LOUISIANA TECH UNIVERSITY

March 2023

LOUISIANA TECH UNIVERSITY

GRADUATE SCHOOL

October 25, 2022
Date of thesis defense

We hereby recommend that the thesis prepared by

Sindhu Datla, B. Pharmacy

entitled **Antimicrobial edible coatings composed of chitosan, polyvinyl alcohol and zinc-coated halloysite nanotubes.**

be accepted in partial fulfillment of the requirements for the degree of

Master of Science in Molecular Sciences and Nanotechnology

David K Mills

Supervisor of Thesis Research

gergana nestorova

Head of Molecular Sciences and Nanotechnology

Thesis Committee Members:
Dr. David Mills
Dr. Gergana Nestorova
Dr. Rebecca Giorno-McConnell

Approved:

Hisham Hegab
Dean of Engineering & Science

Approved:

Ramu Ramachandran
Dean of the Graduate School

GS Form 13
(01/20)

ABSTRACT

Changes in everyday activities like food packaging are required due to the global shift from a linear to a circular economy. Therefore, industrial, and institutional research centers are interested in using biodegradable materials like polyvinyl alcohol and natural raw materials like chitosan to develop novel food packaging films. Edible coating materials have been extensively researched to extend the shelf life of fruits and vegetables and reduce the risk of ingesting chemical reagents. Chitosan (CH) is widely used as a natural preservative for fruits and vegetables, but its poor mechanical, and water resistance limits its use. To improve the properties of chitosan, we prepared chitosan composite films by incorporating polyvinyl alcohol (PVA) with varying amounts of halloysite nanotubes (HNTs) and zinc oxide coated HNTs (ZnHNTs) into a 1% chitosan solution. The effects of PVA/CH blended films with varying concentrations of HNTs and ZnHNTs were assessed using SEM/FESEM, FTIR, and XRD. FTIR and XRD confirmed the presence of zinc on the HNT surface. SEM showed a rough surface that increased roughness with HNT/ZnHNTs addition. Adding ZnHNTs and HNTs improved the chitosan/PVA film's tensile strength (TS) and elongation at break (EAB) with a decrease in light transmittance. We tested the films' antibacterial activity against *Staphylococcus aureus* (*S. aureus*) and *Escherichia coli* (*E. coli*). The CS/PVA/ ZnHNTs films were significantly

antimicrobial over two weeks. Coatings made of PVA and chitosan (80/20 ratio) with concentrations (0, 0.2%, 0.4%, and 0.6%) of HNTs and ZnHNTs were selected for further study. The results indicated that the bio-based films can extend food shelf life and could be used as novel active food packaging materials. Among them, the most promising film was 0.6% ZnHNTs, showing a good preservation effect.

APPROVAL FOR SCHOLARLY DISSEMINATION

The author grants to the Prescott Memorial Library of Louisiana Tech University the right to reproduce, by appropriate methods, upon request, any, or all portions of this Thesis. It is understood that "proper request" consists of the agreement, on the part of the requesting party, that said reproduction is for his personal use and that subsequent reproduction will not occur without written approval of the author of this Thesis. Further, any portions of the Thesis used in books, papers, and other works must be appropriately referenced to this Thesis.

Finally, the author of this Thesis reserves the right to publish freely, in the literature, at any time, any or all portions of this Thesis.

Author _____

Date _____

DEDICATION

This thesis is dedicated to my parents Mr. D. Srinivasa Raju & Mrs. Aruna and my husband Mr. CSK C Varma for their support, belief, love, and encouragement.

TABLE OF CONTENTS

LIST OF FIGURES

LIST OF TABLES

ACKNOWLEDGMENTS

This thesis was possible because of my advisor, Dr. Mills, for his belief in me and his unending encouragement even in dire research circumstances. I acknowledge the help of my lab mates Abdul Razak Masoud and Femi Alakija without whose support it would have been difficult to start in a new lab with such ease.

I would also like to thank Dr. Nestorova and Dr. Giorno for being my committee members. I acknowledge every person who has touched my life in some way and in doing so have contributed to my place here. I hope that this research, a little drop in the vast ocean of science and knowledge, holds the power of infinite possibility.

CHAPTER 1

INTRODUCTION

1.1 Background

1.1.1 Polyvinyl Alcohol

Polyvinyl alcohol, also known as PVA, is a synthetic thermoplastic polymer made by either complete or partial hydrolysis of polyvinyl acetate [1-3]. The molecular weight, particle size distribution, and crystallinity of the polymer chains affect how easily the polymer dissolves in water and other solubility characteristics [2-3]. PVA's molecular weight, concentration, and degree of hydrolysis are just a few variables that significantly impact how well PVA-based polymeric architectures perform [5]. In addition, the polymer is non-toxic, non-carcinogenic, harmless to living tissues, biodegradable, and biocompatible [4]. This polymer is approved by the European Medicine Agency (EMA) and the United States Food and Drug Administration (FDA) for human use. In addition, it can be used as a component of coatings and packaging in food applications.

1.1.2 Chitosan

Chitin is chemically transformed into chitosan, a linear polysaccharide, natural polymer obtained from shells of shrimps and other sea crustaceans [6-8]. Chitosan can dissolve in diluted aqueous acid solutions, such as acetic acid and propionic acid because it has amino groups in its chain. Chitosan has been considered for use in a wide range of industries, including medicine, food, cosmetics, and wastewater treatment, because it is

affordable, non-toxic, and has potentially reactive amino functional groups [10-14]. In addition, this polymer has long been used in the biomedical industry to create various items, including drug delivery systems and hemostatic bandages [8,15-16]. Chitosan, however, has some drawbacks, including low water solubility and a slow capacity for water absorption [17-18]. Therefore, some water-soluble chitosan derivatives, such as chitosan oligosaccharide, chitosan lactate, chitosan succinate, and chitosan glutamate, have been proposed to overcome the limitations mentioned earlier. Chitosan oligosaccharide (COS), produced by the enzymatic or chemical breakdown of chitosan, is a low molecular weight product [19-22]. The antitumor, antibacterial (against *Escherichia coli, Bacillus cereus, and Staphylococcus aureus*), antifungal, anti- inflammatory, antioxidant, and non-toxic properties of COS are among its essential biological attributes [17,21,23]. In addition, the antimicrobial properties of COS can enhance moisture permeability, prevent microbial growth, and promote cell division in wounds [24].

1.1.3 Halloysites

Like kaolinite, halloysite is a naturally occurring clay mineral distinguished by a nanotubular structure. Its chemical formula is $Al_2\ Si_2\ O_5\ (OH)_4\ nH_2O$ [25-26]. HNTs have a 10 to 100 nm internal diameter and an external diameter ranging from 30 to 190 nm [27]. Such nano dimensions are exciting for many reasons. First, HNTs are made primarily of aluminosilicate nano clay and are remarkably adaptable. Second, compared to carbon nanotubes (CNTs), HNTs are a more affordable eco-friendly alternative. Thirdly, due to their exceptional qualities, HNTs have many uses, including plastic and polymer additives, thermoplastics, electronic components, drug delivery, cosmetics, and biomedical applications [28-29]. These composites are not biodegradable despite having good thermal properties. Due to their irregular structure, natural nanotube materials typically disperse quickly. Finally,

HNTs' physicochemical characteristics can be changed [28,30]. HNTs can be added as additives to polymers, which is another characteristic. Additionally, because of their hollow structure, HNTs have the potential to be helpful in a variety of medical applications, including the delivery of drugs and enzymes [31]. For broader applications, it is convenient to obtain uniform nanotube structures [32]. However, it was discovered that even modest HNT loadings significantly altered the polymer properties [27-29]. Particularly sensitive to the polymer's nature is the surface morphology.

1.1.4 Zinc

Zinc can be produced in large quantities using reasonably priced processes and methods, and zinc nanomaterials represent a diverse class of nano products and nano- enabled devices. These nanomaterials also have the potential to have targeted antimicrobial effects and low to negligible phytotoxic effects, making them suitable for direct application and providing powerful antibacterial, antimycotic, antiviral, and antioxygenic activities. Halloysite nanotubes with ZnO nanoparticle coatings can enhance the physicochemical characteristics of biopolymer films and coatings. Even when added in concentrations between 0.1% and 0.6% (w/v %), this oxide metal has demonstrated antimicrobial properties and exhibits high efficacy in preventing the growth of pathogenic microorganisms.

1.2 Chemical Structure of PVA

The degree or extent of polyvinyl acetate's hydrolysis, specifically whether it is complete or partial (Figure 1-1), determines its properties, which in turn determines its classification into two groups, namely (a) partially hydrolyzed and (b) fully hydrolyzed.

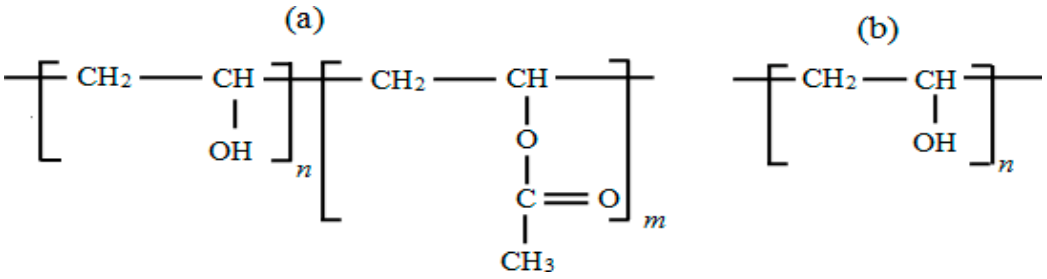

Figure 1-1: Structural formula for PVA: (a) partially hydrolyzed, (b) fully hydrolyzed [33].

The molecular weights obtained for PVA products may differ (20,000-400,000) depending on the length of the initial vinyl acetate polymer, the extent of hydrolysis to remove the acetate groups, and whether it occurs under alkaline or acidic conditions [34]. Figure 1-2 depicts the PVA structure. Hydrolysis levels range from 80%, which is thought to be a typical value, to more than 99%. By cross-linking the linear polymers, nearly fully hydrolyzed forms produce polymer (gel)-fluid (sol) species with tunable properties, which have PVA hydrogels. Low polymer content films produce soft materials because the fluid can freely move through the matrix, whereas high polymer content causes the matrix to stiffen and strengthen significantly [35]. In addition, polymer contents impact the physical status of the resulting material [36].

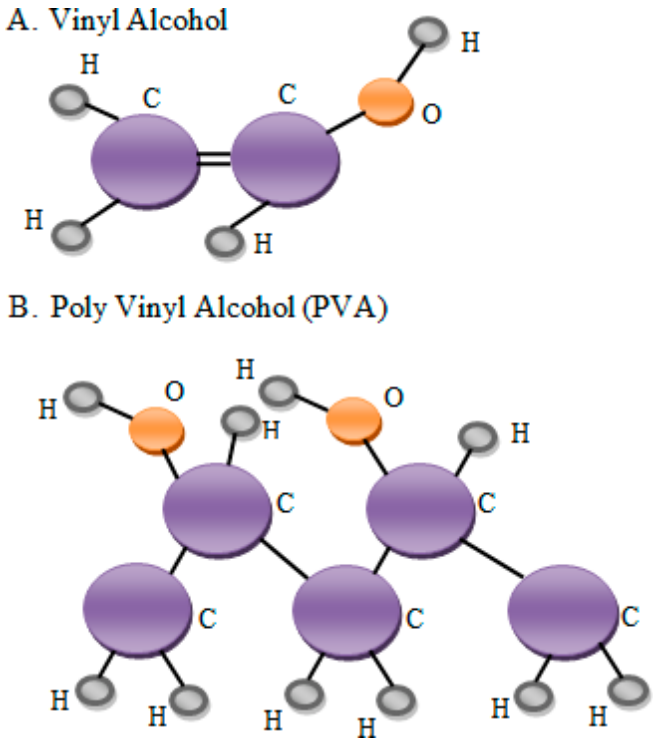

Figure 1-2: The structure of A) vinyl alcohol; B) PVA [37].

1.3 Chemical Structure of Chitosan

A polysaccharide derived from chitin is chitosan. Depending on the chitin's source, its molecular weight ranges from 300 to 1000 kDa [38]. Chitin has a 1-4 linked 2- acetamido-2-deoxy-D-glucopyranose chemical structure (Figure 1-3).

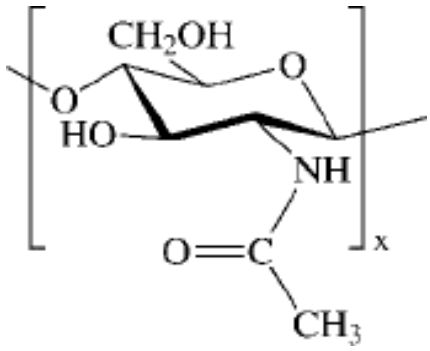

Figure 1-3: Chemical structure of Chitin [38]

As depicted in Figure 1-4, n-acetyl-D-glucose amine and D-glucose amine are copolymers to form chitosan. Chitosan is a linear, semicrystalline [39-40] polymer with at least 60% of the glucose amine residue deacetylated (equals a 60 percent deacetylation degree). Chitin can be deacetylated chemically in highly alkaline conditions or enzymatically in the presence of specific enzymes, including chitin deacetylase [41-42].

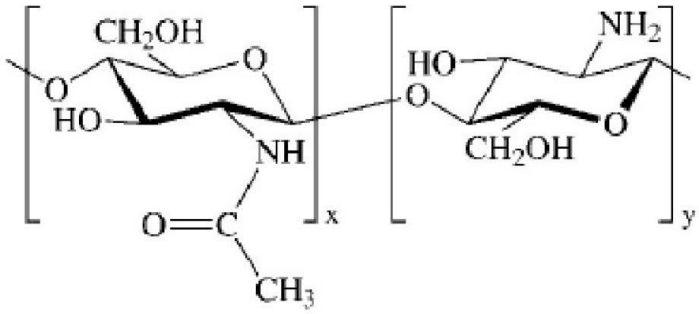

Figure 1-4: Chemical structure of Chitosan [39].

1.4 Chemical Structure of HNTs

HNT micrographs are displayed in Figure 1-5. The halloysites primarily consist of tube-shaped structures and have the following dimensions: The dimensions range from 150 nm to 2 m in length, 20 nm to 100 nm in outer diameter, and 5 nm to 30 nm in lumen diameter. HNTs, due to their distinctive and different morphological characteristics, exhibit unusual charge distributions, surfaces with lower hydroxyl densities, and crystals with

unmatched structures [43]. Tensile strength, optical transmittance, and scanning electron microscopy was used to identify the PVA-HNTs films' distinctive properties [44].

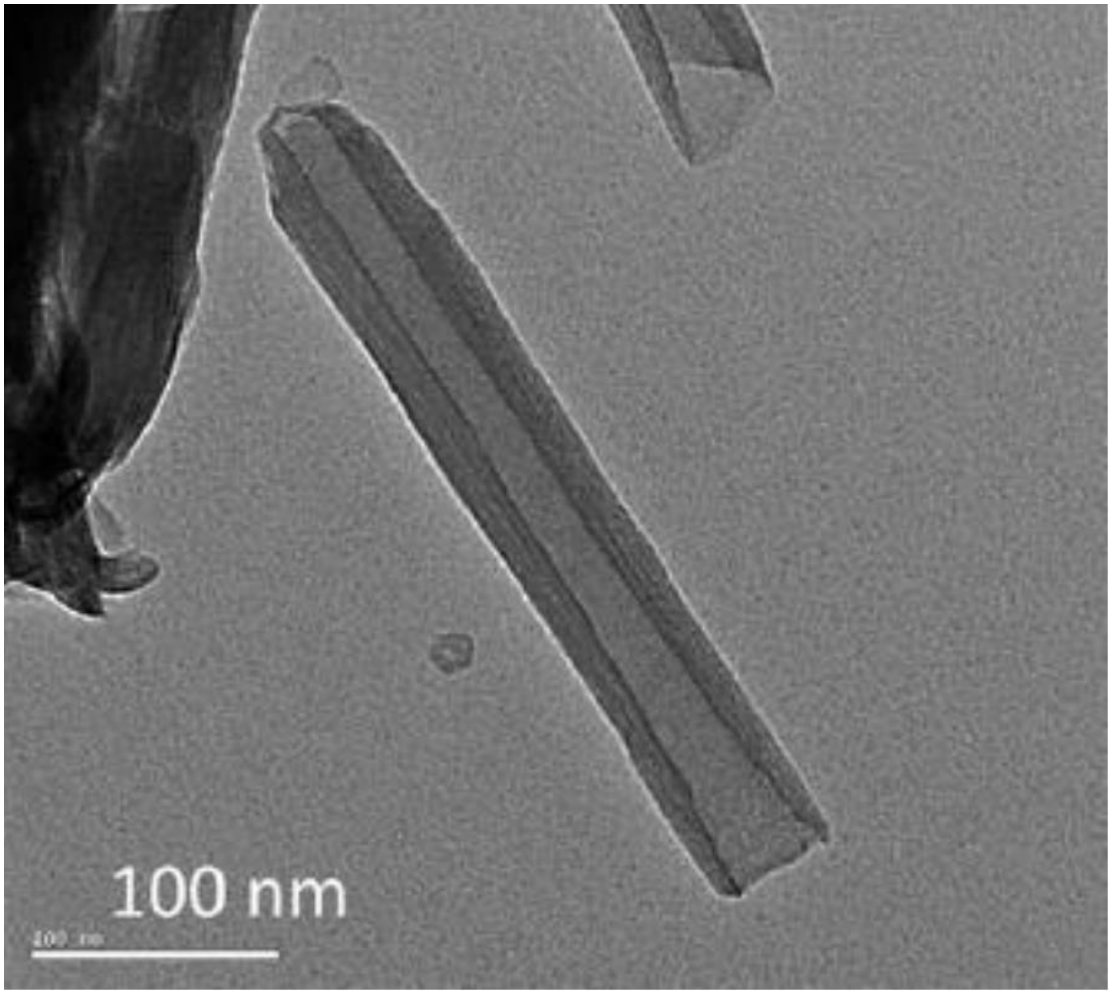

Figure 1-5: TEM micrograph of HNTs [46]

Figure 1-6 depicts a typical crystalline HNT unit with two types of -OH groups and a bilayer structure, with the inner hydroxyl groups located in the shared octahedral (aluminum and oxygen) sheet and the outer hydroxyl groups located in the unshared plane of the tetrahedral (silicon and oxygen) sheet. As a result, siloxanes make up the outside of HNTs, with some silicon hydroxyl groups located in the ends and surface flaws of the HNTs [45]. However, the inner side is where most aluminum hydroxide groups are found. As most of the aluminum hydroxide pairs are located on the inner side of the crystalline formation, and

luminol exhibits a much lower blue shift than the Si-O group [46]. The blue shift of the Si-O stretching FTIR absorption is influenced by the development of H-bonding [47].

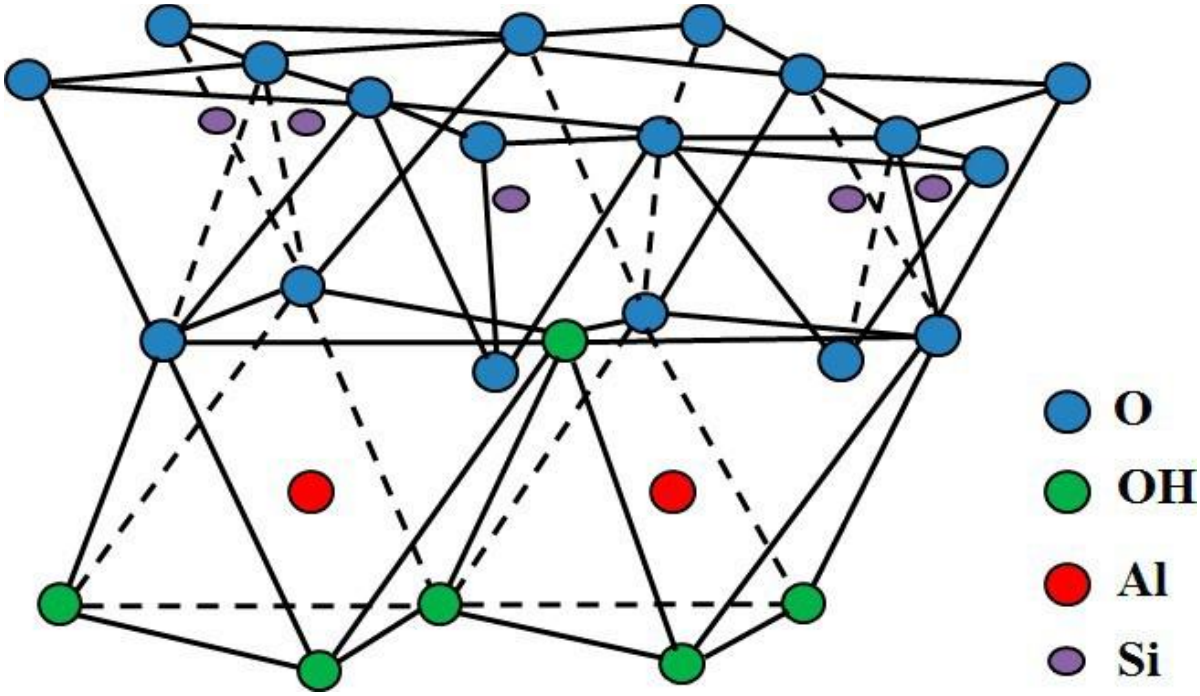

Figure 1-6: Crystalline structure of HNT [48]

CHAPTER 2

MATERIALS AND METHODS

2.1 Materials

Zinc oxide was purchased from Nanostructured & Amorphous Materials Inc. (Katy, TX, USA); HNTs, Chitosan (CS, 200–500 mPa s, degree of deacetylation ≥ 95%) and polyvinyl alcohol (PVA, polymerization degree, 1799; hydrolysis degree, 99%) were purchased from Sigma-Aldrich (St. Louis, MO); DC power source (VWR Accupower 500 electrophoresis power supply), platinum mesh electrodes , and ammeter (Tek Power TP9605BT) were purchased from Amazon.com LLC (Seattle, WA). *Staphylococcus aureus* and *Escherichia coli* were provided by Dr. Rebecca Giorno's lab, Louisiana Tech University.

2.2 Electrolytic Metallization of HNTs

A non-sacrificial standard two-electrode electrolysis setup was assembled consisting of two platinized titanium mesh electrodes acting as cathode and anode, respectively (Figure 2-1). The electrodes were gently cleaned using silicon carbide abrasive papers and washed in distilled water under ultrasonication for 5min to prepare an even surface and to remove any surface contamination. The electrodes were held parallel at a 2-inch distance and connected to a DC power source (VWR Accupower 500 electrophoresis power supply) with an ammeter connected in series (Tek Power TP9605BT) with the setup and connected with a computer via a universal serial bus (USB) connector. The ampere readings were analyzed using Data logger 1.01 software supplied by the manufacturer.

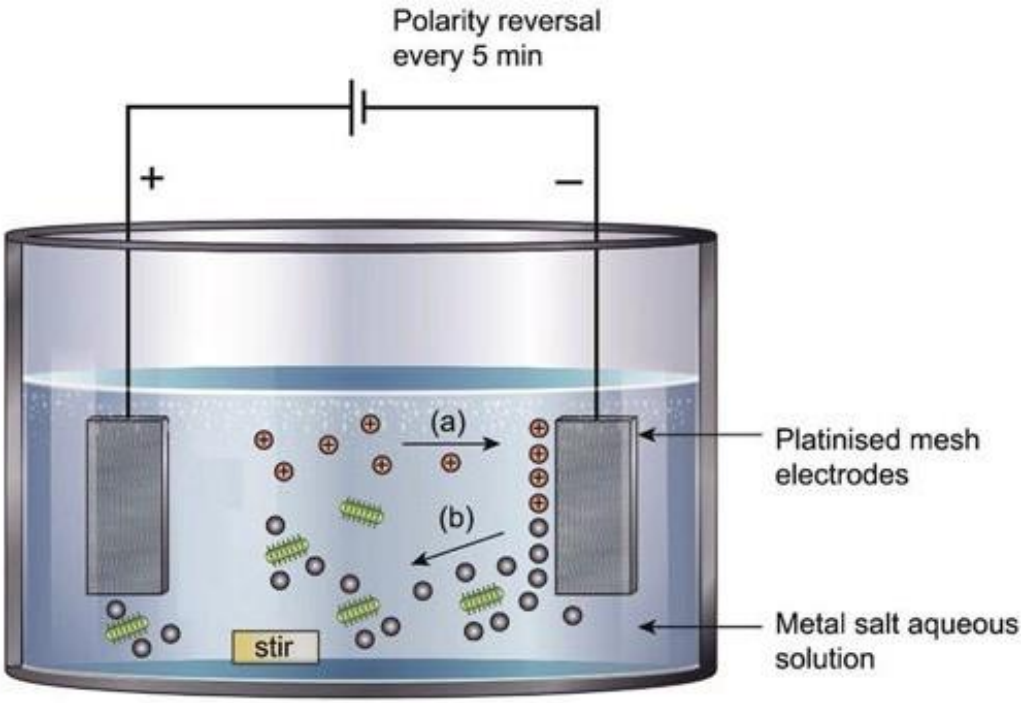

Figure 2-1: Electrolytic Metallization of HNTs [49]

Briefly, an ultrasonicated colloidal solution of 142 mg ZnO and 350 mg HNT in 700 mL of electrolytic solution (water, methanol, or ethanol) was dispersed in the electrolysis vessel (VWR borosilicate glass container). 5, 10, and 20 V Voltages were maintained at 80 °C with equal and opposite polarity reversal at every 5min intervals under constant stirring to reduce electrophoretic buildup and precipitate formation at the working electrode, thus increasing NPS density in the solution (Figure 2-1). Different electrolytic solvents were used to find the optimum solvent with desired conductivity and viscosity balance.

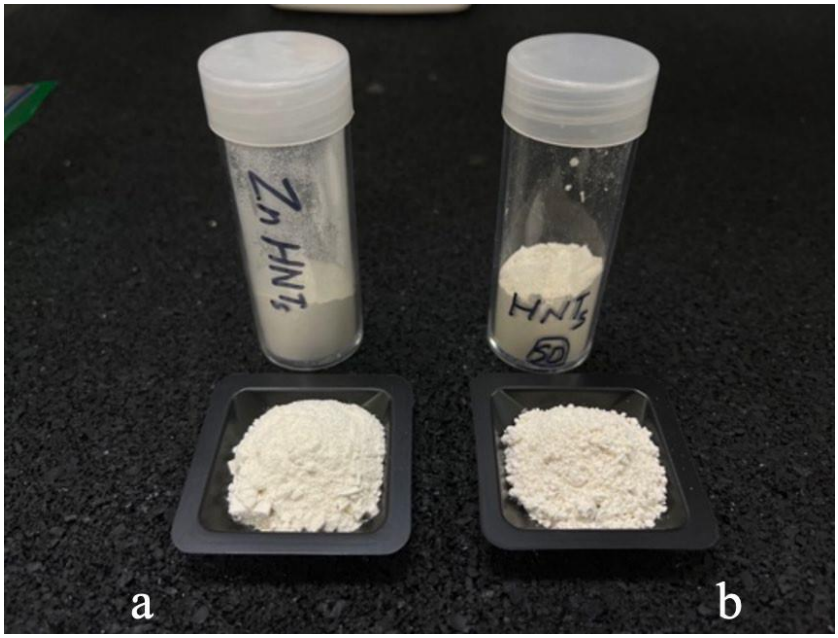

Figure 2-2: a) ZnHNTs after electrolytic metallization b) HNTs purchased from Sigma-Aldrich (St. Louis, MO)

Each set of experiments was carried out for 20min. Afterward, the supernatant was decanted three times, and the solution was centrifuged for 5min at 5000 rpm with water to separate ZnHNTs from the unreacted Zinc NPs and dried at 30 °C (Figure 2-2). The process was optimized for the time duration (5,10, and 20 min), voltage (5,10, and 20 V), and solvent (methanol, ethanol, and water). Multiple batches of each preparation set were created and characterized through the following methods to verify the consistency of the process.

2.3 Preparation of PVA Solution

PVA was dissolved in 500 mL of preheated ultra-pure water to make a 10 g L-1 solution. The mixture was stirred and maintained at roughly 90 ºC for two hours (Figure 2-3).

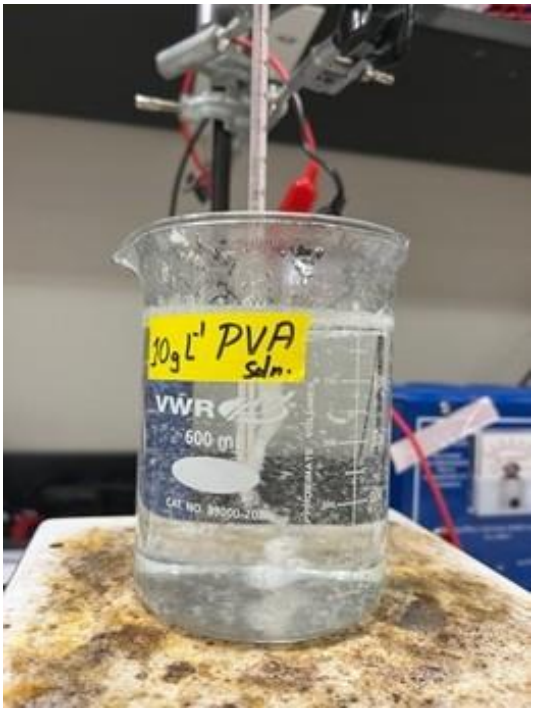

Figure 2-3: Preparation of PVA solution

2.4 Preparation of Chitosan Solution

In an oven, the chitosan was dried until a constant weight was noted. Next, Chitosan was dissolved in 500 mL of acetic acid (0.1 M), stirred, and heated at 60 ºC overnight to create a 10 g L-1 solution (Figure 2-4). The solution was filtered using a filter paper of pore size: 9.0 cm to get rid of dirt and other traces of impurities. The solutions were left at room temperature for two hours to remove air bubbles.

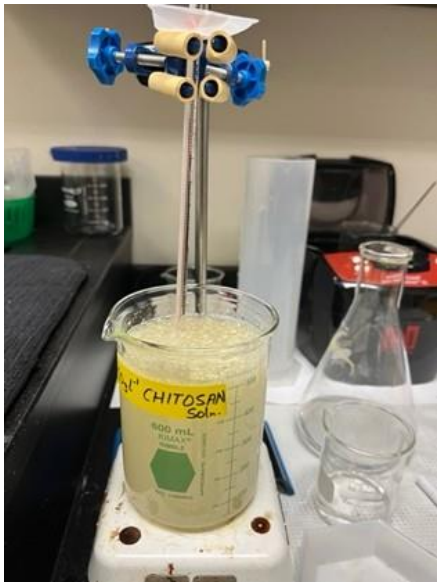

Figure 2-4: Preparation of chitosan solution

2.5 Preparation of Blended Films

Blended films of chitosan and PVA were prepared in ratios of 20 to 80 respectively. Then with constant stirring and a temperature of about 94 °C, the aqueous PVA solution was added drop by drop to the chitosan solution (Figure 2-5). After mixing, stirring was allowed to continue for 30 minutes, and the added PVA to the chitosan solution ranged from 0 to 50 %. Various concentrations (0.2%, 0.4%, and 0.6%) of HNTs and ZnHNTs were added to the solution (Table 2-1). Finally, by pouring standard volume (10 ml) of the resulting homogeneous solutions into polystyrene Petri dishes, followed by 48 hours of drying at 60 °C, films of the solutions were obtained (Figure 2-6).

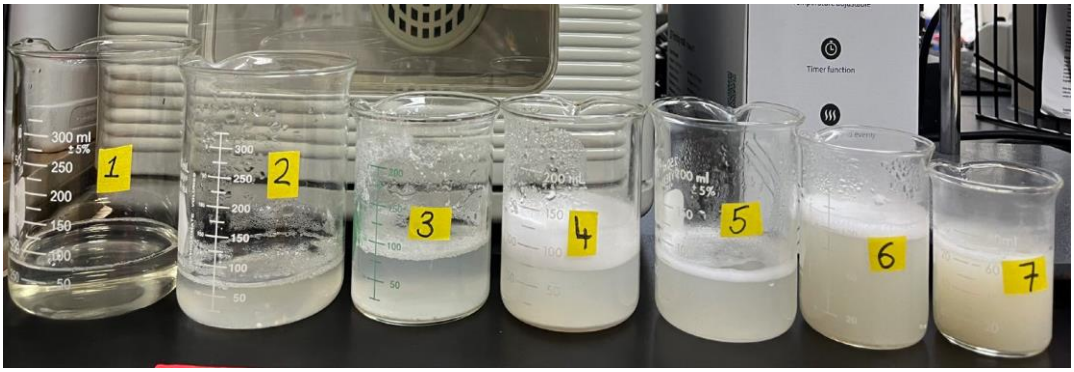

Figure 2-5: Blended film solutions of PVA and Chitosan. 1) PVA/CS (80/20), 2) PVA/CS (80/20) with 0.2% HNTs, 3) PVA/CS (80/20) with 0.4% HNTs, 4) PVA/CS (80/20) with 0.6% HNTs, 5) PVA/CS (80/20) with 0.2% ZnHNTs, 6) PVA/CS (80/20) with 0.4% ZnHNTs 7) PVA/CS (80/20) with 0.6% ZnHNTs.

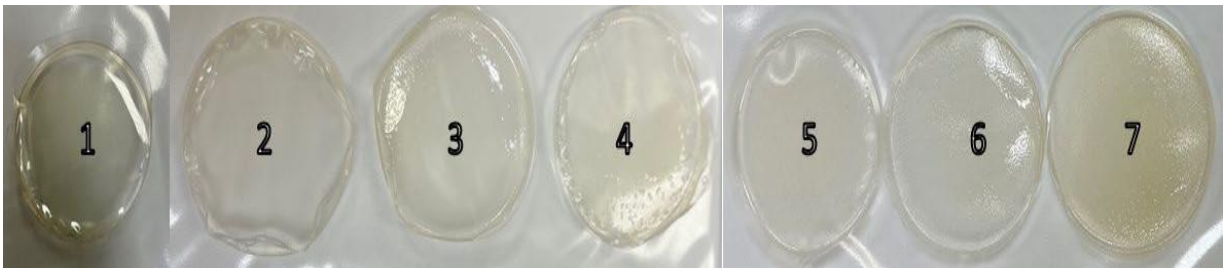

Figure 2-6: Films made of PVA and Chitosan. 1) PVA/CS (80/20), 2) PVA/CS (80/20) with 0.2% HNTs, 3) PVA/CS (80/20) with 0.4% HNTs, 4) PVA/CS (80/20) with 0.6% HNTs, 5) PVA/CS (80/20) with 0.2% ZnHNTs, 6) PVA/CS (80/20) with 0.4% ZnHNTs 7) PVA/CS (80/20) with 0.6% ZnHNTs.

The films were removed, then stored over fresh silica gel in an evacuated desiccator until use. All the obtained films were clear and bubble-free. The same casting process was used to create comparable films from pure chitosan and PVA, which were then used as models. The chitosan films were neutralized overnight with 0.1 M NaOH solution, thoroughly washed with distilled water, and then dried.

Table 2-1: Composition of Films

SAMPLE	PVA/CS	HNTs (wt.%)	ZnHNTs (wt.%)
1	80/20	0	0
2	80/20	0.2 %	0
3	80/20	0.4%	0
4	80/20	0.6%	0
5	80/20	0	0.2%
6	80/20	0	0.4%
7	80/20	0	0.6%

2.6 Scanning Electron Microscopy/Energy Dispersive Spectroscopy (SEM/EDS)

The surface morphology of the coated HNTs was examined using a Hitachi S- 4800 field-emission scanning electron microscope (Tokyo, Japan), which was also used to visually confirm the presence of the metal coating, which appeared as clusters on the otherwise smooth outer surface of the HNTs. To determine the weight percentage of the ZnHNTs constituent elements, SEM-EDS was performed using an EDAX energy dispersive X-ray analyzer connected to the HITACHI S-4800 SEM.EDS was used with an acceleration voltage of 15 kV and a working distance of 15 mm, and the EDAX Genesis software was used to analyze the EDS spectra. The image had 1024 by 768-pixel resolution and a 0.246 by 189-pixel size. The system was set up for EDS element mapping to collect backscatter electrons. In contrast, large spot size and dwell time of 256 μs were used, and the total acquisition time for each sample was 5 minutes.

2.7 X-Ray Diffraction

X-ray crystal diffraction analysis was recorded on a Bruker D8 Venture diffractometer (Bruker, Karlsruhe, German) with Cu Kα1 radiation (λ 1⁄4 1.5418 Å). The

scan speed and step size used were 2s, and 0.02^{O}, respectively, and the diffraction patterns were recorded on a Philips PW 1710 X-ray powder diffractometer over 2θ within3^{O}–50^{O}.

2.8 Attenuated Total Reflection (ATR) Spectroscopy

The Infrared spectrum was recorded at a resolution of $4s^{-1}$ with 16 scans using a Thermo Scientific NICOLET^{TM} IR100 FTIR Spectrometer (Thermo Fisher Scientific; Waltham, MA). In addition, Thermo Scientific OMNICTM software was used to study the stretching bands.

2.9 Tensile Testing

A universal material testing machine was used to measure the tensile strength (TS) and elongation at break (EAB) of the flat, smooth composite films, which were cut into 2.5 cm 8 cm strips (UniVert, universal material testing machine, cell scale). The initial stretching and spacing rates were set at 60 mm per minute for stretching and 5 cm for spacing. The average was calculated from five replicates per sample. The maximum tensile force to cross-sectional area ratio, or TS, was calculated as follows:

$$TS = F_{max}/ (L \times W)$$

Where L is the film's thickness (mm), W is the film's width, and F_{max} is the maximum tensile force (N) (mm).

EAB (%) was determined using the formula:

$$EAB\% = (L1- L0)/L0\ 100\%.$$

L0 denotes the film's initial (mm) length, and L1 is the film's length at the time of breakage (mm).

2.10 Water Solubility

In an oven for 24 hours at 105 ˚C, film pieces (20 × 20 mm) were dried to a constant weight. The films were then submerged in 50 mL of water that was 20 ± 5 ˚C in temperature. Following 24 hours of immersion, the samples were heated to 105 degrees for 24 hours to achieve constant weight. The solubility was determined by:

$$\text{Solubility (\%)} = m_1 - m_2 / m_2 \times 100$$

Where m_1 is the initial weight in grams (g) and m_2 is the final weight in grams (g).

2.11 Antibacterial Activity

The antibacterial properties of HNTs and ZnHNTs on Gram -negative bacteria *Escherichia coli* and Gram -positive bacteria *Staphylococcus aureus* was evaluated. Sample films of 6 mm diameter were sterilized using a UV lamp and placed on Mueller- Hinton inoculated dishes. The diameters of inhibitory zones were measured. Each sample was measured in triplicate, and the average was calculated.

2.11.1 Preparation Of Mueller Hinton Agar

This media is used for the determination of the susceptibility of microorganisms to antimicrobial agents. Suspend 38 grams in 1000ml distilled water, and heat to boiling to dissolve the medium completely. Sterilize by autoclaving at 15lbs pressure (121ºC) for 15 min, cool at 45-45ºC, mix well, and pour into sterile Petri plates.

2.11.2 Preparation Of Mueller Hinton Broth

This is a liquid medium for antibiotic susceptibility studies (MIC-determination). Dissolve 21 grams in 1 liter of distilled water. Sterilize by autoclaving at 121ºC for 15min.

2.11.3 Kirby Bauer Disk Susceptibility Test

In this method, films made of PVA/CS with different concentrations of HNTs and

ZnHNTs were made. The film was then made into a small sample, which weighted the same as the weight of the standard gentamicin discs. The films were impregnated on a Mueller-Hilton agar plate which had the lawn of *E. coli* and *S. aureus* bacteria individually. The inoculation of the bacteria was done when the culture showed an absorbance of 0.08-0.1 at 450 nm. The plates were then incubated at 37 °C for 24 hours. The standards of testing for antibiotics effects are an accepted method by the U.S. Food and Drug Administration and were followed accordingly. The zone of inhibition around the film was measured and noted.

CHAPTER 3

RESULTS AND DISCUSSIONS

3.1 SEM/FESEM

The final films SEM studies revealed that the HNTs and ZnHNTs were uniformly dispersed and that their compatibility with the polymer matrix had been significantly improved the smoothness. When compared to the other films, which appear to have slightly rougher surfaces and homogeneous morphologies, the structure of the raw PVA/CS surface matrices after cross-section studies is smoother. As a result, the size of the zinc crystallite is considerably smaller, and the sizes estimated by the XRD measurements are accurate (Figure 3-2). Furthermore, it can be assumed that the ZnHNTs are hidden in photos 7, 8, and 9 due to their smaller sizes or the presence of Zinc ions from their homogeneous dissolution in the PVA/CS matrix.

Different surface morphologies were visible in the SEM images of the pure PVA/CS and composite films with different HNT and ZnHNTs concentrations. The smoothness of the composite film surface vanished because of HNTs and ZnHNTs accumulating and dispersing over the surface of the pure PVA and chitosan film. In contrast, the surface of the pure PVA and chitosan film had a uniform surface and texture (Figure 3-1). These findings indicated that the two polymer materials were complementary and that the HNT and ZnHNTs additions altered the film structure. As a result of the fixation effect caused by the interaction between PVA/CS film and Zinc, it has been reported that there were uniform Zn protrusions in the

composite films [50]. Additionally, the addition of ZnHNTs has been reported to interfere with chitosan's molecular structure and affect its mechanical properties, leading to slight changes to its surface morphology [51]. The addition of ZnHNTs may improve the mechanical strength of films due to the formation of electrostatic bonds between chitosan and Zn particles that cause the film surface to be rough [52].

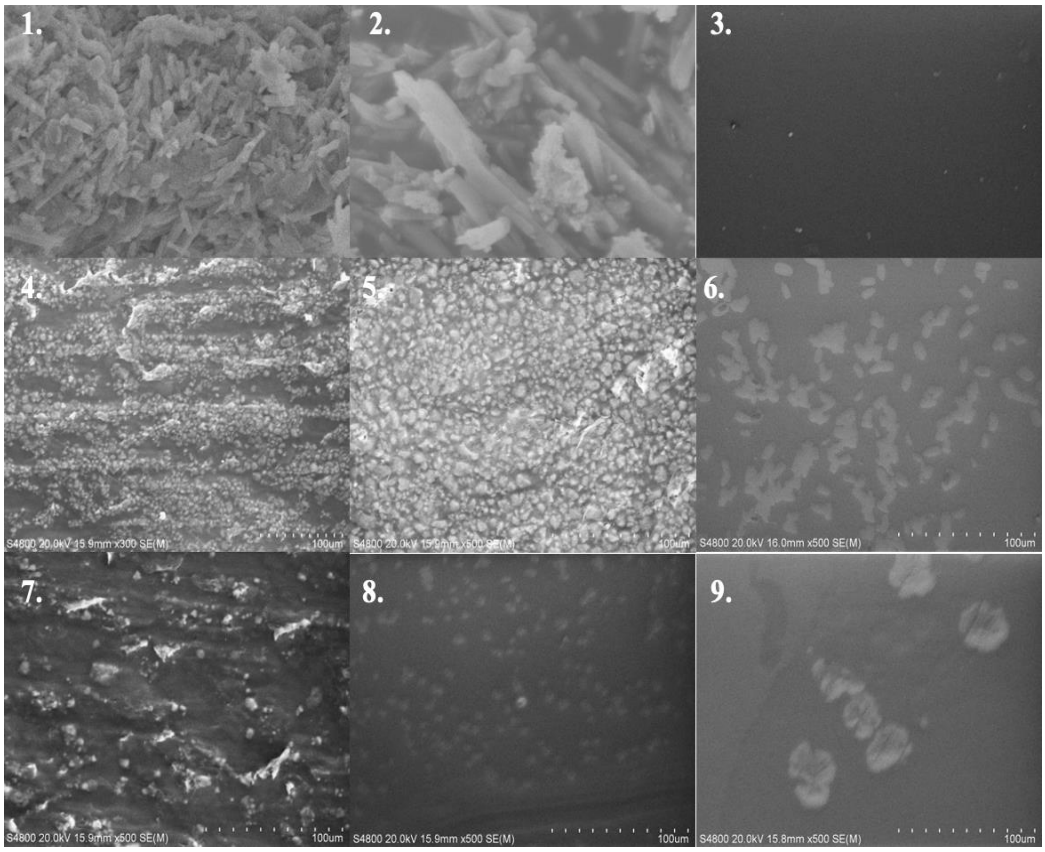

Figure 3-1: FESEM/SEM 1) HNTs 2) ZnHNTs 3) PVA/CS (80/20), 4) PVA/CS (80/20) with 0.2% HNTs, 5) PVA/CS (80/20) with 0.4% HNTs, 6) PVA/CS (80/20) with 0.6% HNTs, 7) PVA/CS (80/20) with 0.2% ZnHNTs, 8) PVA/CS (80/20) with 0.4% ZnHNTs 9) PVA/CS (80/20) with 0.6% ZnHNTs.

SEM images were taken to verify the existence of coatings and the ideal temperature for coating the HNTs. Zn was applied as a coating to the HNTs images at 80°C. Figure 3-2 illustrates the HNTs' Zn coating, which is uneven but complete. Figure 3-1 (1) illustrates how HNTs, by default, have a smoother exterior. Halloysite attracts positively charged ions to form a

bond that can either be a Van der Waals bond or a weak ionic bond because it has an opposing exterior surface due to the presence of OH. The Zn+2 binds to the HNTs' surface in both situations.

To confirm Zn's presence on the HNTs, an EDAX analysis—a quantitative examination of the chemical elements in a chosen area—was carried out. As shown in Figure 3-1 (1) and (2), the EDS-SEM examined the chemical characterization of the region chosen on HNTs and ZnHNTs. The HNT and ZnHNTs elemental reports quantitative analysis of the various elements clarifies that Zn-on-Zn coated HNTs exist. However, the reports of ZnHNTs do not show the precise Si peak. As a result, since Si's K shell peak overlaps Zn's L shell peak, the value is 0. Figure 3-2 displays all the samples of HNTs and the average of the qualitative compositional data for HNTs and ZnHNTs. EDAX confirmed the presence of Zn, adding value to the coating method for ZnHNTs. It also estimates their population size. Other elements, such as overlapping peaks, may impact this method's accuracy. Therefore, additional tests were carried out to estimate the sample composition more accurately. For the HNTs and ZnHNTs, as well as for the various films with various compositions, EDAX images and elemental analysis were observed. The Zn element is present inside the extremely well-homogenized films, as shown by the surface mapping's estimate of 0.6% Zn and the cross-section mapping's estimate of 0.3% Zn. It is also evident from the surface and cross-section analyses. It lends strong support to the findings of the antimicrobial measurements, which could show that the ZnHNTs materials exhibit enhanced antimicrobial activity compared to the pertinent HNT materials.

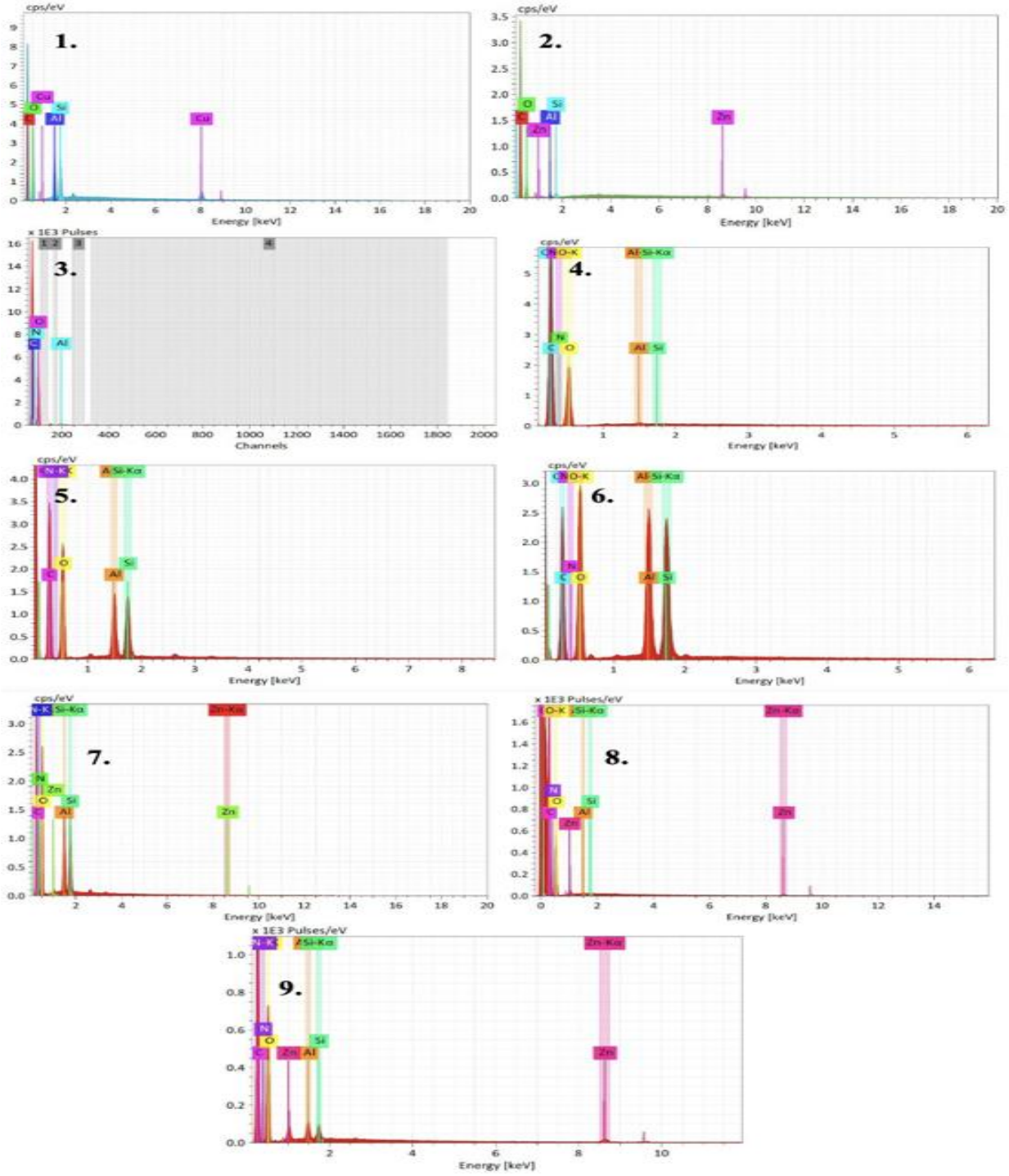

Figure 3-2: EDAX 1) HNTs 2) ZnHNTs 3) PVA/CS (80/20), 4) PVA/CS (80/20) with 0.2% HNTs, 5) PVA/CS (80/20) with 0.4% HNTs, 6) PVA/CS (80/20) with 0.6% HNTs, 7) PVA/CS (80/20) with 0.2% ZnHNTs, 8) PVA/CS (80/20) with 0.4% ZnHNTs 9) PVA/CS (80/20) with 0.6% ZnHNTs

3.2 XRD

Figure 3-3 displays the pure HNT and ZnHNTs X-ray diffraction patterns in the 2theta angle range of 2theta = 2° to 2theta = 40°. The peak's growth suggests that the HNTs are well-oriented, and zinc coated. The size of ZnHNTs and HNTS peaks was calculated using the theory of Williamson and Hull [53] and the methodology outlined elsewhere [54] and was discovered to be 64.9 nm and 37.5 nm, respectively. It is known that the antimicrobial activity of such ZnHNTs depends on the crystal size.

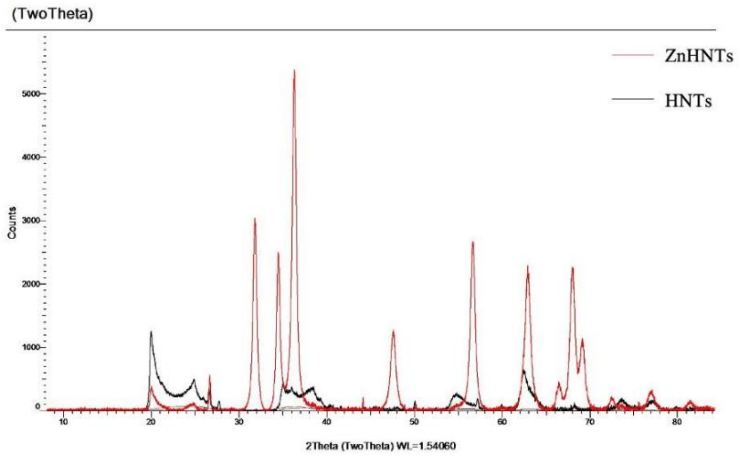

Figure 3-3: The XRD Patterns of HNTs and ZnHNTs powder

The semi-crystalline nature of chitosan was demonstrated by the XRD patterns of pure chitosan (Figure 3-4 a) and PVA powders (Figure 3-4 b), which appeared at 19.9. The XRD pattern of PVA/CS films with varying concentrations of HNTs and ZnHNTs is shown in Figure 3-5. The characteristic peaks were observed at 31.6, 34.3, 36.2, 47.5, 56.5, 62.8, and 67.8, which corresponded to the (1 0 0), (002), (0 0 1), (1 0 2), (1 1 0), (10 3), and (2 0 1) planes of PVA/CS (80/20), PVA/CS (80/20) with 0.2% HNTs, PVA/CS (80/20) with 0.4% HNTs, PVA/CS (80/20) with 0.6% HNTs, PVA/CS (80/20) with 0.2% ZnHNTs, PVA/CS (80/20) with 0.4% ZnHNTs, PVA/CS (80/20) with 0.6% ZnHNTs, respectively.

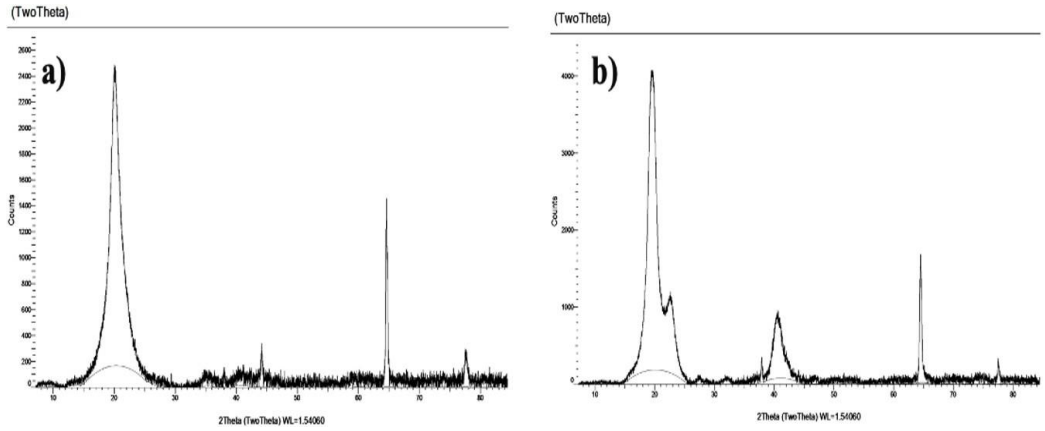

Figure 3-4: The XRD Patterns of a) Chitosan and b) PVA powder

Higher zinc content in the composite film resulted in a more recognizable ZnHNTs peak. The XRD patterns of the following materials are shown in Figure 3-5: PVA/CS (80/20), PVA/CS (80/20) with 0.2% HNTs, 0.4% HNTs, 0.6% HNTs, PVA/CS (80/20) with 0.2% ZnHNTs, 0.4% ZnHNTs, and 0.6% ZnHNTs. Wide reflections can be seen in the pure CS sample (Figure 3-4 a) and PVA sample, respectively, at 10° and 19.9°. This pattern points to the presence of tiny and damaged crystals. The peak of neat CS at a 2theta angle of about 10° almost completely vanishes in the case of the PVA/CS blend film. This peak shift suggests that the PVA molecules expand the free space in the CS chain and result from chain interactions between CS and PVA. When HNTs are added to the PVA/CS blend, the 001 reflection shifts from 7.3° to 5.2° for different HNT concentrations and from 11.9° to 9.3° for different ZnHNTs concentrations. These shifts indicate the formation of intercalated nanocomposite structures in the lower angles.

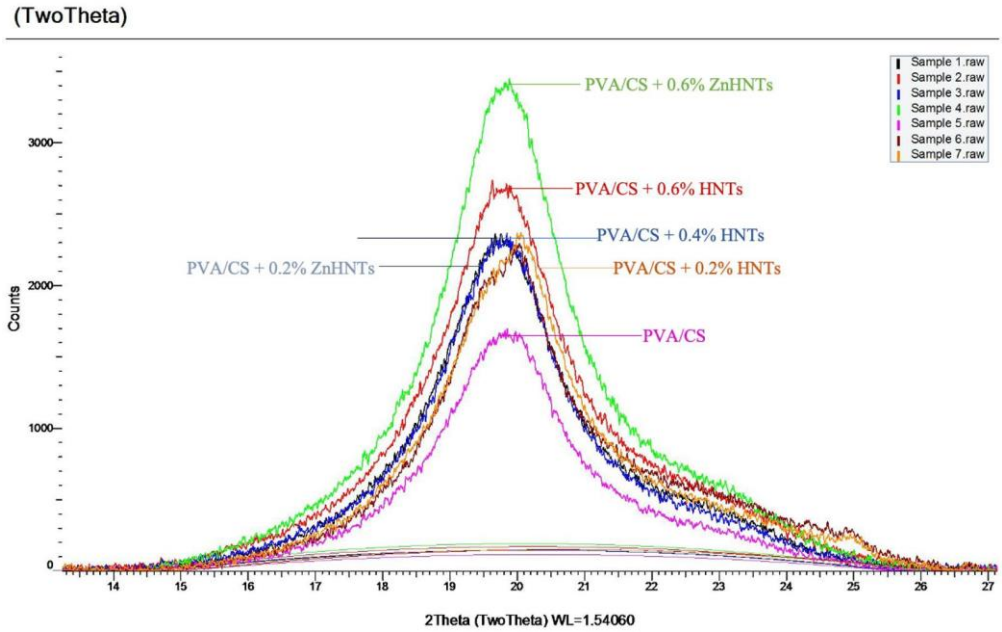

Figure 3-5: XRD 1) PVA/CS (80/20), 2) PVA/CS (80/20) with 0.2% HNTs, 3) PVA/CS (80/20) with 0.4% HNTs, 4) PVA/CS (80/20) with 0.6% HNTs, 5) PVA/CS (80/20) with 0.2% ZnHNTs, 6) PVA/CS (80/20) with 0.4% ZnHNTs, 7) PVA/CS (80/20) with 0.6% ZnHNTs.

Additionally, PVA and Chitosan were seen at the low angle region of all XRD plots (Figure 3-4), around 7.3° and 11.9°, respectively. No differences were found when comparing the basal space of the HNTs with the corresponding different concentrations of HNTs and the basal space of the ZnHNTs with the corresponding concentrations of ZnHNTs. These facts show that the interlayer space between the HNTs and the HNTs with Zn concentrations did not change.

3.3 FTIR

The FTIR spectra of HNTs and ZnHNTs are shown in Figure 3-6, and they both exhibit a distinctive absorption band at 3626 cm^{-1}, which denotes the stretching of the OH group bonded to the Al3+ cation. Additionally, it displays a distinctive band at 3442 cm1, which is attributed to the H2O stretching vibrations. In Figure 3-7, the H2O bending vibrations are represented by the band at 1641 cm1, while the SiO stretching vibrations are represented by the bands at 1113 cm^{-1}

and 1031 cm1. Additionally, the bands at 913 cm1 indicate the Al-OH bending mode, while the peaks at 879, 913, and 844 cm1 are bands of OH bending modes.

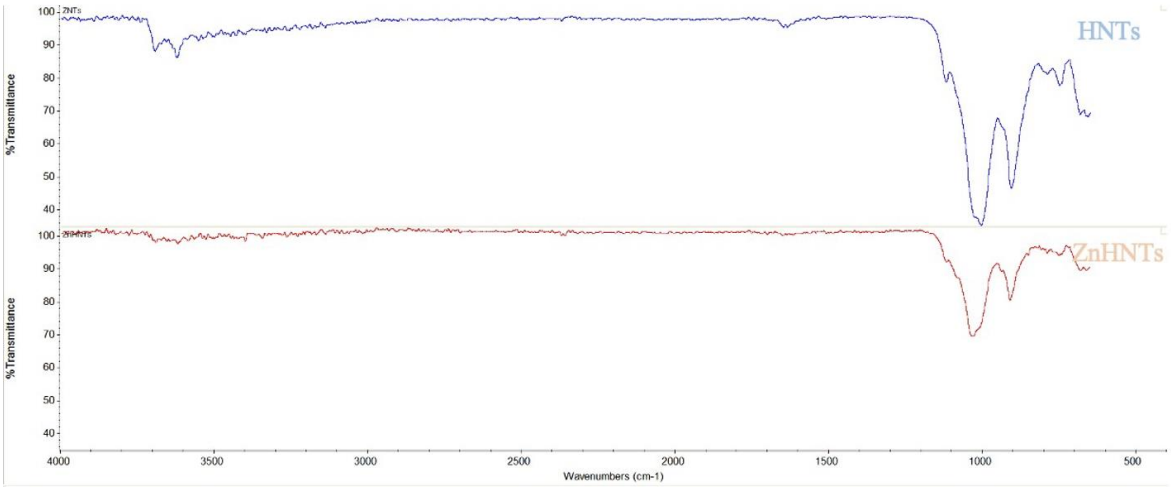

Figure 3-6: FTIR plots of a) HNTs and b) ZnHNTs

Al Zn-bending OH's mode is shown by the band at 879 cm1, while the band shows Zn-bending OH's mode at 844 cm1. The band indicates the stretching vibration of the inner surface OH groups at 3695 cm1 of the HNT FTIR spectrum. The band at 3622 cm -1 represents the inner group stretching vibration. This is because hydrogen bonds were created between the inner surface OH groups and the oxygen sheets. These OH groups are also linked to the sheets of octahedra with an Al center. Therefore, it is possible to see two bands that should appear at approximately 3650 cm^{-1} and 3670 cm^{-1} and are typical of the inner surface OH groups of halloysite.

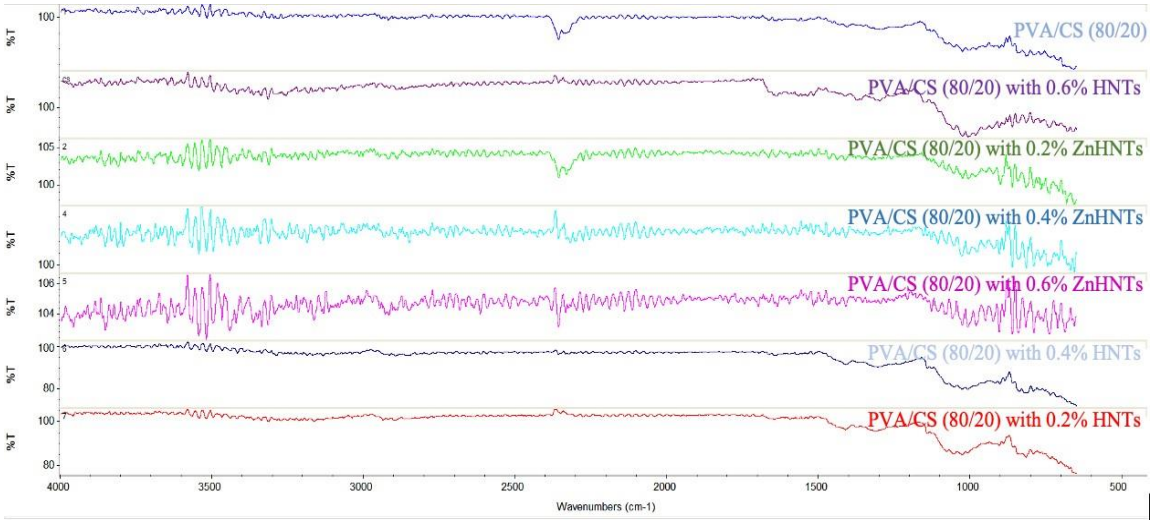

Figure 3-7: FTIR plots of 1) PVA/CS (80/20), 2) PVA/CS (80/20) with 0.2% HNTs, 3) PVA/CS (80/20) with 0.4% HNTs, 4) PVA/CS (80/20) with 0.6% HNTs, 5) PVA/CS (80/20) with 0.2% ZnHNTs, 6) PVA/CS (80/20) with 0.4% ZnHNTs 7) PVA/CS (80/20) with 0.6% ZnHNTs

The spectra of HNTs and ZnHNTs at various concentrations (Figure 3-7) show an absorption band at about 520 cm1. Pure zinc exhibits this band, which is typical and distinctive. The absorption band indicates the O-H mode at 3434 cm1. The 0.2% and 0.4% HNT peaks were also diminished in both FTIR spectra. This fact suggests that Zn was formed on the exterior of HNT. Two distinct peaks were present at 1553 cm-1 and 1394 cm-1, indicating the symmetric stretching of the carboxylate group (COO), which is most likely the result of a small amount of zinc leftover from the coating process.

3.4 Tensile Testing

As shown in Figure 3-8, the TS and EAB values of pure PVA/CS film were 43.65 ± 1.50 MPa and 5.19 ± 0.28%, respectively. In contrast, those of composite films containing different concentrations of nano-ZnO were in the ranges 33.74 ± 2.13–46.79 ± 1.68 MPa and 7.66 ± 0.66–13.26 ± 0.41%, respectively. Compared with the pure PVA/CS film, the TS values of composite films containing 0.2% and 0.4% HNTs and ZnHNTs decreased by

26.57%,1.21%, and 28.13%, 2.23%, respectively (Figure 3-8), while that of the composite films containing 0.6% HNTs and ZnHNTs increased by 4.82% 6.68%, respectively. The TS values of composite films containing 0.4% and 0.6% HNTs and ZnHNTs differed significantly. The EAB values of composite films containing 0.6% HNTs and ZnHNTs were significantly higher) then those of the pure PVA/CS film than composite films containing 0.2% and 0.4% HNTs and ZnHNTs. The EAB values of composite films containing 0.2%, 0.4%, and 0.6% HNTs and ZnHNTs increased by 30.84%, 40.39%, 140.86%, and 31.65%,41.22%,150.11% respectively (Figure 3-8). Thus, the addition of ZnHNTs enhanced the TS of the films. It can be concluded that the TS and EAB values of PVA/CS films increased by adding 0.2%-0.6% Zn (Table 3-1). These findings can be explained by forming strong new bonds between PVA, chitosan, and Zn due to nanoparticle matrix interface interactions. The addition of Zn to HNTs can generate an intermolecular cross-linking effect. The interface bonding between PVA/CS and Zn with HNTs results in the effective transfer of stress to the particles, which can improve the mechanical properties of the composite film.

Table 3-1: Tensile Testing

Sample	**Tensile strength (TS)**	**Elongation of break (EAB)**
PVA/CS	43.65 ± 1.50	5.19 ± 0.28
PVA/CS + 0.2% HNTs	33.88 ± 2.01	11.12 ± 0.45
PVA/CS + 0.4% HNTs	37.12 ± 1.62	9.34 ± 0.56
PVA/CS + 0.6% HNTs	42.98 ± 1.45	7.01 ± 0.58
PVA/CS + 0.2% ZnHNTs	34.74 ± 2.33	13.36 ± 0.41
PVA/CS + 0.4% ZnHNTs	38.81 ± 2.01	10. 28 ± 0.60
PVA/CS + 0.8% ZnHNTs	46.79 ± 1.68	7.66 ± 0.66

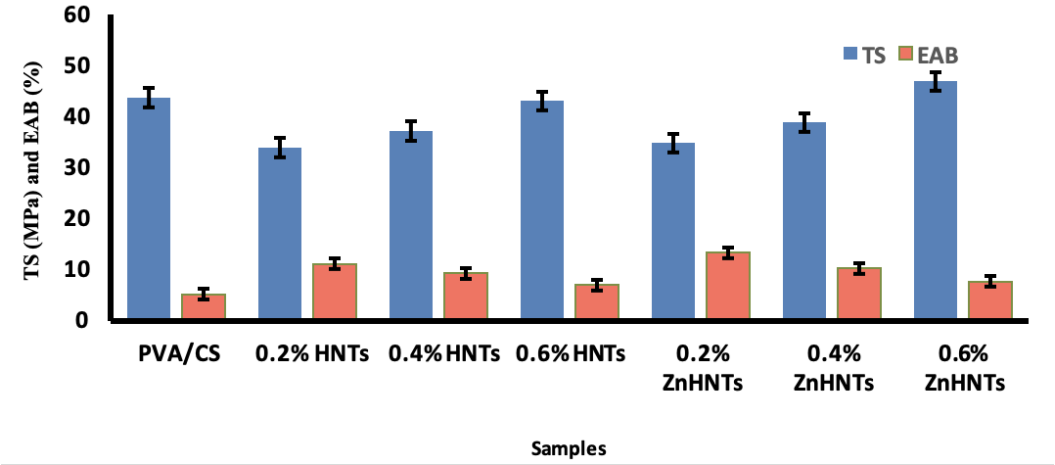

Figure 3-8: Tensile strength and Elongation of break

3.5 Water Solubility

In the composite film containing PVA/CS, 0.2% HNTs, 0.4% HNTs, 0.6% HNTs, 0.2% ZnHNTs, 0.4% ZnHNTs, and 0.6% ZnHNTs, the water solubility values were 25.41.25%, 22.15 1.2%, 19.75 2.2%, 18.45 0.98%, 21.12 0.2, 16.98 1.1%, and 12.34 1. The outcomes showed that adding HNTs and ZnHNTs gradually reduced the PVA/CS film's water solubility. This might be brought on by weakening the interaction between the hydrophilic groups on the PVA and chitosan chain and the surrounding molecules due to the cross-linking of Zn and HNTs with the hydrophilic groups.

3.6 Antibacterial Activity

By taking an accurate measurement of the clear inhibition zone's diameter, the inhibitory activity was assessed. The diameter was defined as zero when there was no surrounding clear zone because it was assumed there was no inhibitory zone. The film was then made into a small sample, which weighted the same as the weight of the standard gentamicin discs (Figure 3-9). The effect of HNT and ZnHNTs was tested for 24 hours on the growth rate of two bacteria, *Escherichia coli* and *Staphylococcus aureus*, separately. ZnHNTs

increased zone of inhibition in the case of two bacteria compared to HNT. It showed that HNT had an inherent property with some bactericidal or bacteriostatic effect on bacteria, which was enhanced when HNT was coated with Zinc. ZnHNTs have some inherent quality that lowers the bacterial growth rate. In our study, it was noted that PVA/CS with ZnHNTs films (Table 3-2) exhibited better antimicrobial activity in comparison to PVA/CS and PVA/CS with HNTs films.

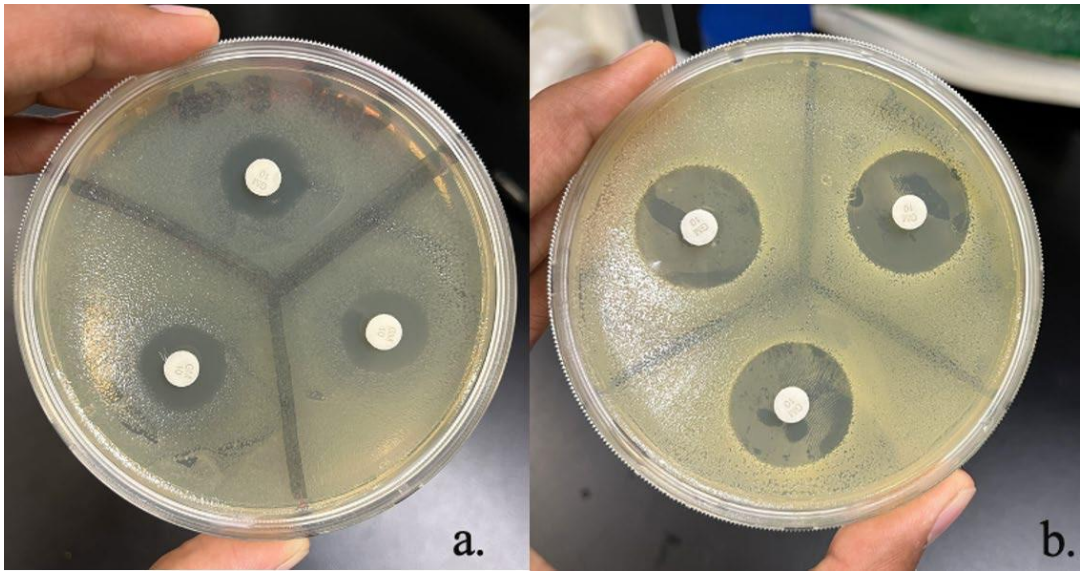

Figure 3-9: Gentamicin Discs a) *E. coli* b) *S. aureus*.

It is well known that chitosan has some antimicrobial properties, which are thought to be the result of an interaction between the positively charged amino glucose units' ammonium (NH4+) and the negatively charged components of the bacterial cell wall. Due to this interaction, the bacterial outer membrane degrades, allowing vital intracellular components to leak out and negatively affecting the function of bacterial cells, ultimately resulting in cell death [55]. However, because pure CS has poor mechanical properties, this issue is fixed by blending it with other polymers, like PVA. Furthermore, PVA shows resistance to acidic and alkaline conditions [56], whereas CS loses its antibacterial activity in

non-acidic conditions. Thus, this polymer combination improves the final films mechanical and, in most cases, antimicrobial properties. PVA and Chitosan have broad-spectrum antibacterial properties and high film-forming stability, which microorganisms can degrade. Adding ZnHNTs to the PVA and chitosan composite film significantly enhanced its antibacterial effects. The inhibition zone diameters in different strains are shown in (Figures 3-10 and 3-11). The inhibition zones of pure PVA and chitosan film against *E. coli and S. aureus* measured 0.00mm and 0.00mm, respectively. Chitosan binds to the cell membrane and eliminates the barrier function of Gram-positive bacteria by creating porous structures on their surfaces.

Additionally, chitosan enters Gram-negative bacteria to adsorb its ionic components and disrupt metabolism, preventing bacterial growth. The zones of inhibition of the two tested bacteria grew compared to pure PVA, and chitosan film as the amount of ZnHNTs increased, depending on the ZnHNTs concentration. Compared to the pure PVA and chitosan film, the antimicrobial activity of composite films containing 0.6% ZnHNTs revealed a discernible difference between the two strains (Figure 3-10, 3-11).

Table 3-2: Treatment groups for combined drug therapy.

Film Material	***E. coli* Inhibition Zone*** **(Mean Diameter of Clear Zone in mm)**	***S. aureus* Inhibition Zone*** **(Mean Diameter of Clear Zone in mm)**
PVA/CS (80/20)	0.00	0.00
PVA/CS (80/20) with 0.2% HNTs	0.00	0.00
PVA/CS (80/20) with 0.4% HNTs	0.01	0.00
PVA/CS (80/20) with 0.6% HNTs	0.02	0.00
PVA/CS (80/20) with 0.2% ZnHNTs	6.00	3.25
PVA/CS (80/20) with 0.4% ZnHNTs	7.50	4.75
PVA/CS (80/20) with 0.6% ZnHNTs	8.50	5.50

* Inhibitory zone surrounding film discs measured in mm after the subtraction of the disc diameter (6 mm).

Concerning the surrounding clear zone, the PVA/chitosan films used as control did not show any migrated inhibitory activity against *E. coli* and *S. aureus*. However, when HNTs were added, they did show an antibacterial effect underneath the films where no bacterial growth was observed.

The inhibition zones of *E. coli* and *S. aureus* were significantly increased by adding 0.6% ZnHNTs to 8.50mm and 5.50mm, respectively. The composite film's antibacterial effect was stronger against *E. coli* than against *S. aureus*. This might be brought on by the *S. aureus* cell wall's substantial layer of peptide glycans [61]. ZnHNTs are a powerful antibacterial substance that appears to significantly enhance the antibacterial properties of the PVA and chitosan film. In ZnHNTs composite films, ZnO can potentially have a synergistic effect by increasing the positive charges of the chitosan amino group, which in turn improves interactions with the negatively charged microbial cell wall [62]. These reports show that zinc ions are necessary for normal bacterial cell function. As a result, low concentrations of ZnO may stimulate bacteria's intracellular metabolic processes, while high concentrations of zinc are toxic to them. However, zinc affects bacterial pathogenesis, biofilm formation, intracellular growth, and other aspects of bacterial behavior in a complex and contradictory way.

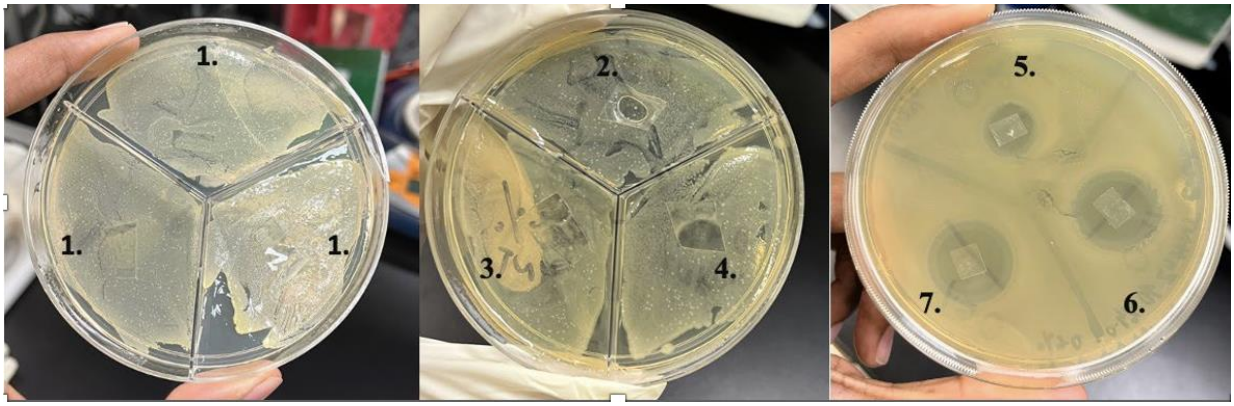

Figure 3-10: Antibacterial activity on *E. coli* 1) PVA/CS (80/20), 2) PVA/CS (80/20) with 0.2% HNTs, 3, 4) PVA/CS (80/20) with 0.6% HNTs, 5) PVA/CS (80/20) with 0.2% ZnHNTs, 6) PVA/CS (80/20) with 0.4% ZnHNTs 7) PVA/CS (80/20) with 0.6% ZnHNTs.

Considering the HNT and ZnHNTs-based films, the PVA/CS with 0.6% ZnHNTs film demonstrated higher antibacterial activity against all tested bacteria compared to the PVA/CS with different concentrations of HNTs and ZnHNTs. In addition, the inhibitory zones were noticeably higher for PVA/CS with 0.6% ZnHNTs films. Against Gram- positive and Gram-negative bacteria, including foodborne pathogens like *E. coli*, *Salmonella enterica spp*., *L. monocytogenes*, and *S. aureus*, ZnO nanoparticles appear to have a wide range of antibacterial activities [57,58]. By making better and closer contact with the bacteria cells, ZnO nanoparticles can easily disrupt the functions of their membranes. Additionally, the reduced bacterial growth and elevated nanocomposite concentration are related. The nanoparticles produced a significant amount of reactive oxygen species under visible light when they were more effectively attached to the bacteria membrane. The ability to provide a larger external surface area and subsequently more active sites to produce more reactive oxygen species is thus possible when ZnO nanoparticles show higher dispersion. Singlet oxygen may oxidize the cell's contents, leading to bacterial disorganization [59].

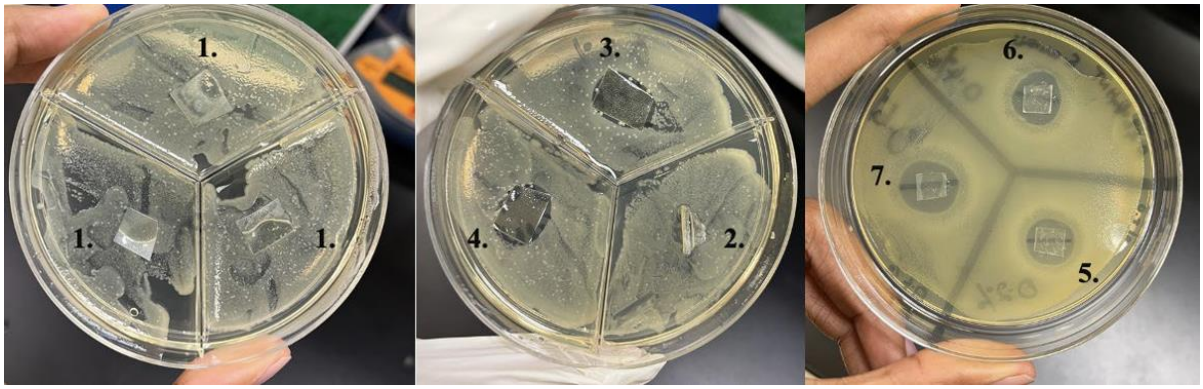

Figure 3-11: Antibacterial activity on *S. aureus* 1) PVA/CS (80/20), 2) PVA/CS (80/20) with 0.2% HNTs, 3, 4) PVA/CS (80/20) with 0.6% HNTs, 5) PVA/CS (80/20) with 0.2% ZnHNTs, 6) PVA/CS (80/20) with 0.4% ZnHNTs 7) PVA/CS (80/20) with 0.6% ZnHNTs.

It is important to note that the combined effects of CS, PVA, HNTs, and ZnHNTs are undoubtedly responsible for the final effectiveness of the studied films against the tested bacteria. Additionally, the bacterial strain, nanoparticle type/size, growth media type, and bacterial cell concentration are all linked to the antimicrobial activity of any given nanostructure [60]. For future experiments, the composite film containing 0.6% ZnHNTs can be used because it exhibits the best antibacterial performance.

CHAPTER 4

DISCUSSION

4.1 Discussion

In this study, we created composite films made of PVA and chitosan that contained varying amounts of HNTs and ZnHNTs, and we assessed their mechanical, water-soluble, and antibacterial qualities. We demonstrated the compatibility of PVA, chitosan, HNTs, and Zn; ZnHNTs can enhance the tensile strength, elongation of break, and antibacterial activity of PVA/CS films. Regarding antibacterial activity against *S. aureus* and *E. coli*, the composite film containing 0.6% HNTs was the most effective. The Zn material brings this on, partially dissolved as Zn2+ ions in the PVA/CS matrix and partially well-oriented on the external surface of the HNTs. By using XRD and SEM, the properties of the final, ideal composite films were quantified. Due to the strong intermolecular hydrogen bonding between the amino groups of chitosan and the hydroxyl groups of PVA, the properties of the obtained blends showed good miscibility between chitosan and PVA, as shown by the results of FTIR, FESEM, and SEM. This was anticipated given the smaller crystal size that the XRD measurements calculated and the over-double Zn content that the SEM-EDX measurements estimated. The XRD spectra also demonstrated the intercalation of HNTs by the PVA/CS composite material, which results in perfectly homogeneous

final films, as shown by the FTIR measurements and the SEM images. Due to chitosan's hydrophilicity, this is typical. The tensile measurements revealed that they also exhibited enhanced mechanical characteristics. The SEM images clearly show that the fine dispersion of the Zn onto HNTs is the cause of these improved mechanical properties. Compared to the pure PVA and chitosan film, all blended films had significantly lower water uptake, suggesting that the hydrophilicity has improved. These outcomes further demonstrated the success of the PVA and chitosan composite film preparation.

4.2 Future Work

Fruit and vegetable quality is associated with management and climatic conditions during production. Therefore, it is necessary to use other processes for everyday consumption to prevent microbiological deterioration and minimize the physiological and biochemical changes that occur post-harvest, including degradation [61-63]. Fruit and vegetable packaging is designed to avoid microbial decline and reduce the physiological and biochemical changes responsible for post-harvest degradation. Plastic packaging derived from petroleum presents severe environmental problems, including degradation, environmental impact, and effects on animal, human and ecological health [63,64].Significant losses can be observed during, and after harvest, possibly due to mechanical damage, inadequate storage, transport conditions, and sale display that favor contamination of fungi and bacteria [65,66].

The design in films and coatings applied to fruits and vegetables reduces the loss of moisture, lipids, and aromas, improves oxygen barrier properties, and enhances coating adhesion and durability [67-69]. Edible skin coatings are under intense

research due to the public's increasing demand for high-quality, low-cost, nutritious fruits and vegetables [69]. There is also a critical societal need to minimize disposable packaging waste and improve waste management, thus reducing the environmental impact of current packing material [70]. Furthermore, edible surface coatings in packaged foods can provide an invisible physical barrier to oxygen, external microbial contamination, and moisture absorption/desorption [71-73]. Recently, edible coatings functionalized with bioactive compounds, such as natural antimicrobial compounds, antioxidants, minerals, vitamins, and aromatics, have also been developed [74,75]. This research can preserve food quality, handle, and deliver greater health benefits to the consumer [74-76].

Deep space missions and future occupants of Lunar and Mars habitats will also require a means for long-term storage of plant crops. Edible plant coatings with an extended shelf life that preserves food quality and taste will make fruits more attractive and significantly improve the meal experience. Also critical is fruit and vegetable packaging used to prevent microbiological deterioration and minimize the physiological and biochemical changes responsible for post-harvest degradation [77]. New technologies must be developed that ensure food quality, increase shelf life, and have a low environmental impact [78].

REFERENCES

[1] Qureshi D, Sahoo A, Mohanty B, Anis A, Kulikouskaya V, Hileuskaya K, Agabekov V, Sarkar P, Ray SS, Maji S, Pal K. Fabrication, and characterization of poly (vinyl alcohol) and chitosan oligosaccharide-based blend films. Gels. 2021 Jun;7(2):55.

[2] Kang Y, Wu X, Chen Q, Ji X, Bo S, Liu Y. Adsorption of poly (vinyl alcohol) on gel permeation chromatography columns depends on the degree of hydrolysis. Journal of Chromatography A. 2019 Jan 25; 1585:138-43.

[3] Tampau A, González-Martínez C, Chiralt A. Polyvinyl alcohol-based materials encapsulating carvacrol obtained by solvent casting and electrospinning. Reactive and Functional Polymers. 2020 Aug 1; 153:104603.

[4] Gaaz TS, Sulong AB, Akhtar MN, Kadhum AA, Mohamad AB, Al-Amiery AA. Properties and applications of polyvinyl alcohol, halloysite nanotubes and their nanocomposites. Molecules. 2015 Dec 19;20(12):22833-47.

[5] Zhang H. Ice templating and freeze-drying for porous materials and their applications. John Wiley & Sons; 2018 Oct 22.

[6] Lee JY, Termsarasab U, Lee MY, Kim DH, Lee SY, Kim JS, Cho HJ, Kim DD. Chemosensitizing indomethacin-conjugated chitosan oligosaccharide nanoparticles for tumor-targeted drug delivery. Acta biomaterialia. 2017 Jul 15; 57:262-73.

[7] De Queiroz Antonino RS, Lia Fook BR, de Oliveira Lima VA, de Farias Rached RÍ, Lima EP, da Silva Lima RJ, Peniche Covas CA, Lia Fook MV. Preparation and characterization of chitosan obtained from shells of shrimp (Litopenaeus vannamei Boone). Marine drugs. 2017 May 15;15(5):141.

[8] Nageh H, Ezzat M, Ghanim M, Hassanin A, Abd El-Moneim A. Evaluation of antibacterial activity and drug release behavior of chitosan-based nanofibers (in vitro study). Pharmaceutical and Biosciences Journal. 2014 Jun 22:01-5.

[9] El-Hefian EA, Nasef MM, Yahaya AH. The preparation and characterization of chitosan/poly (vinyl alcohol) blended films. E-journal of chemistry. 2010 Oct 1;7(4):1212-9.

[10] Khor E, Lim LY. Implantable applications of chitin and chitosan. Biomaterials. 2003 Jun 1;24(13):2339-49.

[11] Xin-Yuan S, Tian-Wei T. New contact lens based on chitosan/gelatin composites. Journal of Bioactive and Compatible Polymers. 2004 Nov;19(6):467-79.

[12] Crini G. Non-conventional low-cost adsorbents for dye removal: a review. Bioresource Technology. 2006 Jun 1;97(9):1061-85.

[13] Araki C, Arai K, Hirase S. Studies on the chemical constitution of agar-agar.XXIII. Isolation of D-xylose, 6-O-methyl-D-galactose, 4-O-methyl-L-galactose and O-methylpentose. Bulletin of the Chemical Society of Japan. 1967 Apr;40(4):959-62.

[14] Stephen AM, Phillips GO. Food polysaccharides and their applications. CRC press; 2016 Apr 19.

[15] Bae KH, Park M, Do MJ, Lee N, Ryu JH, Kim GW, Kim C, Park TG, Hyeon T. Chitosan oligosaccharide-stabilized ferrimagnetic iron oxide nanocubes for magnetically modulated cancer hyperthermia. ACS nano. 2012 Jun 26;6(6):5266- 73.

[16] Kean T, Thanou M. Biodegradation, biodistribution and toxicity of chitosan. Advanced drug delivery reviews. 2010 Jan 31;62(1):3-11.

[17] Fernandez-de Castro L, Mengíbar M, Sánchez Á, Arroyo L, Villarán MC, de Apodaca ED, Heras Á. Films of chitosan and chitosan-oligosaccharide neutralized and thermally treated: Effects on its antibacterial and other activities. Lwt. 2016 Nov 1; 73:368-74.

[18] Termsarasab U, Cho HJ, Kim DH, Chong S, Chung SJ, Shim CK, Moon HT, Kim DD. Chitosan oligosaccharide–arachidic acid-based nanoparticles for anti-cancer drug delivery. International journal of pharmaceutics. 2013 Jan 30;441(1-2):373- 80.

[19] Jiang Z, Li H, Qiao J, Yang Y, Wang Y, Liu W, Han B. Potential analysis and preparation of chitosan oligosaccharides as oral nutritional supplements of cancer adjuvant therapy. International journal of molecular sciences. 2019 Feb 20;20(4):920.

[20] Kumar A, Kumar A. Fabrication of eggshell membrane–based novel buccal mucosa–mimetic surface and mucoadhesion testing of chitosan oligosaccharide films. Journal of Materials Research. 2019 Nov;34(22):3777-86.

[21] Naveed M, Phil L, Sohail M, Hasnat M, Baig MM, Ihsan AU, Shumzaid M, Kakar MU, Khan TM, Akabar MD, Hussain MI. Chitosan oligosaccharide (COS): An overview. International journal of biological macromolecules. 2019 May 15; 129:827-43.

[22] Guan G, Azad MA, Lin Y, Kim SW, Tian Y, Liu G, Wang H. Biological effects and applications of chitosan and chito-oligosaccharides. Frontiers in physiology. 2019 May 7; 10:516.

[23] Mahato KK, Sabbarwal S, Misra N, Kumar M. Fabrication of polyvinyl alcohol/chitosan oligosaccharide hydrogel: physicochemical characterizations and in vitro drug release study. International Journal of Polymer Analysis and Characterization. 2020 Jul 3;25(5):353-61.

[24] Mengíbar M, Mateos-Aparicio I, Miralles B, Heras Á. Influence of the physico- chemical characteristics of chito-oligosaccharides (COS) on antioxidant activity. Carbohydrate polymers. 2013 Sep 12;97(2):776-82.

[25] Joussein E, Petit S, Churchman J, Theng B, Righi D, Delvaux B. Halloysite clay minerals—a review. Clay minerals. 2005 Dec;40(4):383-426.

[26] Abdullayev E, Lvov Y. Halloysite clay nanotubes as a ceramic “skeleton” for functional biopolymer composites with sustained drug release. Journal of materials chemistry B. 2013;1(23):2894-903.

[27] Ismail H, Pasbakhsh P, Fauzi MA, Bakar AA. Morphological, thermal, and tensile properties of halloysite nanotubes filled ethylene propylene diene monomer (EPDM) nanocomposites. Polymer Testing. 2008 Oct 1;27(7):841-50.

[28] Shchukin D, Moehwald H. Self-repairing coating containing active nanoreservoirs. Small 2007; 3:926–43.

[29] Ye Y, Chen H, Wu J, Ye L. High impact strength epoxy nanocomposites with natural nanotubes. Polymer. 2007 Oct 5;48(21):6426-33.

[30] Cavallaro G, Lazzara G, Milioto S. Dispersions of nanoclays of different shapes into aqueous and solid biopolymeric matrices. Extended physicochemical study. Langmuir. 2011 Feb 1;27(3):1158-67.

[31] Wei W, Abdullayev E, Hollister A, Mills D, Lvov YM. Clay nanotube/poly (methyl methacrylate) bone cement composites with sustained antibiotic release. Macromolecular materials and engineering. 2012 Jul;297(7):645-53.

[32] Ali MA, Zulfiqar AZ, Arif AM, Khan AR, Masih S, Iqbal Z. Edible skin coating material containing neither ammonia nor morpholine. Journal of Postharvest Technology. 2017;5(1):43-54.

[33]. Gaaz TS, Sulong AB, Akhtar MN, Kadhum AA, Mohamad AB, Al-Amiery AA. Properties and applications of polyvinyl alcohol, halloysite nanotubes and their nanocomposites. Molecules. 2015 Dec 19;20(12):22833-47.

[34] DeMerlis CC, Schoneker DR. Review of the oral toxicity of polyvinyl alcohol (PVA). Food and chemical Toxicology. 2003 Mar 1;41(3):319-26.

[35] Tan CJ, Tong YW. The effect of protein structural conformation on nanoparticle molecular imprinting of ribonuclease a using miniemulsion polymerization. Langmuir. 2007 Feb 27;23(5):2722-30.

[36] Yang JM, Su WY, Yang MC. Evaluation of chitosan/PVA blended hydrogel membranes. Journal of Membrane Science. 2004 Jun 15;236(1-2):39-51.

[37] Baker MI, Walsh SP, Schwartz Z, Boyan BD. A review of polyvinyl alcohol and its uses in cartilage and orthopedic applications. Journal of Biomedical Materials Research Part B: Applied Biomaterials. 2012 Jul;100(5):1451-7.

[38] Bhardwaj N, Kundu SC. Electrospinning: a fascinating fiber fabrication technique. Biotechnology advances. 2010 May 1;28(3):325-47.

[39] Arya SK, Manohar M, Singh G, Siddiqui WA. Chitin and chitosan-complexes and their applications. Chitosan: Derivatives, Composites and Applications. 2017 Aug 18:151-65.

[40] Croisier F, Jérôme C. Chitosan-based biomaterials for tissue engineering. European polymer journal. 2013 Apr 1;49(4):780-92.

[41] Rinaudo M. Chitin and chitosan: Properties and applications. Progress in polymer science. 2006 Jul 1;31(7):603-32.

[42] Jayakumar R, Menon D, Manzoor K, Nair SV, Tamura H. Biomedical applications of chitin and chitosan-based nanomaterials—A short review. Carbohydrate polymers. 2010 Sep 5;82(2):227-32.

[43] Venkatesan J, Kim SK. Chitosan composites for bone tissue engineering—an overview. Marine drugs. 2010 Aug 2;8(8):2252-66.

[44] Tang Y, Zhou D, Zhang J. Novel polyvinyl alcohol/styrene butadiene rubber latex/carboxymethyl cellulose nanocomposites reinforced with modified halloysite nanotubes. Journal of Nanomaterials. 2013 Jan 1;2013.

[45] Ng KW, Wanivenhaus F, Chen T, Hsu HC, Allon AA, Abrams VD, Torzilli PA, Warren RF, Maher SA. A novel macroporous polyvinyl alcohol scaffold promotes chondrocyte migration and interface formation in an in vitro cartilage defect model. Tissue Engineering Part A. 2012 Jun 1;18(11-12):1273-81.

[46] Lin Y, Ng KM, Chan CM, Sun G, Wu J. High-impact polystyrene/halloysite nanocomposites prepared by emulsion polymerization using sodium dodecyl sulfate as surfactant. Journal of colloid and interface science. 2011 Jun 15;358(2):423-9.

[47] Stasio, F.D.; Korniychuk, P.; Brovelli, S.; Uznanski, P.; McDonnell, S.O.; Winroth, G.; Anderson, H.L.; Tracz, A.; Cacialli, F. Highly Polarized Emission from Oriented Films Incorporating Water-Soluble Conjugated Polymers in a Polyvinyl Alcohol Matrix. *Adv. Mater.* **2011**, *23*, 1855–1859.

[48] Du M, Guo B, Lei Y, Liu M, Jia D. Carboxylated butadiene–styrene rubber/halloysite nanotube nanocomposites: Interfacial interaction and performance. Polymer. 2008 Oct 17;49(22):4871-6.

[49] Humayun A, Mills D. Voltage regulated electrophoretic deposition of silver nanoparticles on halloysite nanotubes. Results in Materials. 2020 Sep 1;7:100112.

[50] Malini M, Thirumavalavan M, Yang WY, Lee JF, Annadurai G. A versatile chitosan/ZnO nanocomposite with enhanced antimicrobial properties. International journal of biological macromolecules. 2015 Sep 1; 80:121-9.

[51] Mittal H, Ray SS, Kaith BS, Bhatia JK, Sharma J, Alhassan SM. Recent progress in the structural modification of chitosan for applications in diversified biomedical fields. European Polymer Journal. 2018 Dec 1; 109:402-34.

[52] Liu Y, Cai Y, Jiang X, Wu J, Le X. Molecular interactions, characterization, and antimicrobial activity of curcumin–chitosan blend films. Food Hydrocolloids. 2016 Jan 1; 52:564-72.

[53] Williamson GK, Hall WH. X-ray line broadening from filed aluminium and wolfram. Acta metallurgica. 1953 Jan 1;1(1):22-31.

[54] Makarona E, Koutzagioti C, Salmas C, Ntalos G, Skoulikidou MC, Tsamis C. Enhancing wood resistance to humidity with nanostructured ZnO coatings. Nano- Structures & Nano-Objects. 2017 Apr 1; 10:57-68.

[55] Shahidi F, Arachchi JK, Jeon YJ. Food applications of chitin and chitosans. Trends in food science & technology. 1999 Feb 1;10(2):37-51.

[56] Cazón P, Velazquez G, Ramírez JA, Vázquez M. Polysaccharide-based films, and coatings for food packaging: A review. Food Hydrocolloids. 2017 Jul 1; 68:136- 48.

[57] Jones N, Ray B, Ranjit KT, Manna AC. Antibacterial activity of ZnO nanoparticle suspensions on a broad spectrum of microorganisms. FEMS microbiology letters. 2008 Feb 1;279(1):71-6.

[58] Liu YJ, He LL, Mustapha A, Li H, Hu ZQ, Lin MS. Antibacterial activities of zinc oxide nanoparticles against Escherichia coli O157: H7. Journal of applied microbiology. 2009 Oct;107(4):1193-201.

[59] Shu Z, Zhang Y, Yang Q, Yang H. Halloysite nanotubes supported Ag and ZnO nanoparticles with synergistically enhanced antibacterial activity. Nanoscale Research Letters. 2017 Dec;12(1):1-7.

[60] Bagchi B, Kar S, Dey SK, Bhandary S, Roy D, Mukhopadhyay TK, Das S, Nandy P. In situ synthesis and antibacterial activity of copper nanoparticle loaded natural montmorillonite clay based on contact inhibition and ion release. Colloids and Surfaces B: Biointerfaces. 2013 Aug 1; 108:358-65.

[61] Muraleedaran K, Mujeeb VA. Applications of chitosan powder within situ synthesized nano ZnO particles as an antimicrobial agent. International Journal of Biological Macromolecules. 2015 Jun 1; 77:266-72.

[62] Rahman PM, Mujeeb VA, Muraleedharan K. Flexible chitosan-nano ZnO antimicrobial pouches as a new material for extending the shelf life of raw meat. International journal of biological macromolecules. 2017 Apr 1; 97:382-91.

[63] Ncube, L.K.; Ude, A.U.; Ogunmuyiwa, E.N.; Zulkifli, R.; Beas, I.N. Environmental impact of food packaging materials: a review of contemporary development from conventional plastics to Polylactic Acid Based Materials. Materials 2020, 13, 4994. https://doi.org/10.3390/ma13214994.

[64] Nkwachukwu, O.I., Chima, C.H., Ikenna, A.O. *et al.* Focus on potential environmental issues in plastic world towards a sustainable plastic recycling in developing countries. Int J Ind Chem 2013; 4(34) (2013). https://doi.org/10.1186/2228-5547-4-34.

[65] Murmu, SB., Mishra, H. N. Engineering evaluation of thickness and packaging materials based on the modified atmosphere packaging requirements of guava (Cv. Baruipur). LWT-Food Science and Technology, 2018; 78, 273–280.

[66] Wikstrom, F., Williams, H., & Venkatesh, G. (2016). The influence of packaging attributes on recycling and food waste behavior - An environmental comparison of two packaging alternatives. Journal of Cleaner Production, 2016; 137, 895–902.

[67] Del-Valle, V., Hernandez-Munoz, P., Guarda, A. and Galotto M. J., 2005. Development of a cactus-mucilage (Opuntia ficus indica) edible coating and its application to extend strawberry (Fragaria ananassa) shelf-life. Food Chemistry. 91(4):751–756.

[68] Lin, D., and Zhao Y. 2007. Innovation in the development and application of edible coatings for fresh and minimally processed fruits and vegetables. Comprehensive Reviews in Food Science and Food Safety. 6(3):60–75.

[69] Hambleton, A., Fabra, M. J., Debeaufort, F., Dury-Brun, C. and Voilley, A. 2009. Interface and aroma barrier properties of iota carrageenan emulsion-based films used to encapsulate active food compounds. Journal of Food Engineering. 93:80– 88.

[70] Olivas, G. I., Barbosa-Cánovas, G. V. 2009. Edible films and coatings for fruits and vegetables. In: Edible Films and Coatings for Food Applications. (Eds. M.E. Embuscado and Huber K.C.). Springer Science, LLC., New York, USA, pp. 211244.

[71] Vargas, M., Pastor, C., Chiralt, A., McClements, D.J. and Gonzalez-Martinez, C. 2008. Recent advances in edible coatings for fresh and minimally processed fruits. Critical Reviews in Food Science and Nutrition. 48: 496–511.

[72] Aoron, H; Zaitzev, Y; Porat, R; Powvernov, E. 2014. Effects of carboxymethyl cellulose and chitosan bilayer edible coating on postharvest quality of citrus fruit. Postharvest Biology and Technology 87: 21-26.

[73] Dhall, RK. 2013. Advances in edible coatings for fresh fruits and vegetables: a review. Critical Reviews in Food Science and Nutrition 53: 435-50.

[74] Ali, M.A., Zulfiqar, A.Z., Arif, A.M., Khan, A.R., Masih, S. and Iqbal, Z. 2017. Edible skin coating material containing neither ammonia nor morpholine. Journal of Postharvest Technology, 5(1): 43-54.

[75] Tavassoli-Kafrani, E., Shekarchizadeh, H., & Masoudpour-Behabadi, M. (2016). Development of edible films and coatings from alginates and carrageenans. Carbohydrate Polymers, 137, 360–374.

[76] Joussein E, et al. Halloysite Clay Minerals: A Review. Clay Min. 2005; 40:383– 426.

[77] Abdullayev E, Lvov, L. Halloysite clay nanotubes as a ceramic "skeleton" for functional biopolymer composites with sustained drug release. J. Mater. Chem. B, 2013:1:2894–2903.

[78] Ismail H, Pasbakhsh P, Fauzi AMN, Abu Bakar A. Morphological, thermal, and tensile properties of halloysite nanotubes filled ethylene propylene diene monomer (EPDM) nanocomposites. Polymer Testing 2008; 27:841–50.